Preprints.org

Article

Not peer-reviewed version

Large-Range Switchable Asymmetric Transmission and Circular Conversion Dichroism in a VO_2 Based Metasurface

Songliang Zhao , Huan Jiang * , Jingyu Wang , Wenchang Zhu , Weiren Zhao

Posted Date: 14 July 2023

doi: 10.20944/preprints202307.0958.v1

Keywords: Active Metasurface; Phase change materials; Chiral effects; Dynamic polarization control

Preprints.org is a free multidiscipline platform providing preprint service that is dedicated to making early versions of research outputs permanently available and citable. Preprints posted at Preprints.org appear in Web of Science, Crossref, Google Scholar, Scilit, Europe PMC.

Copyright: This is an open access article distributed under the Creative Commons Attribution License which permits unrestricted use, distribution, and reproduction in any medium, provided the original work is properly cited.

Preprints (www.preprints.org) | NOT PEER-REVIEWED | Posted: 14 July 2023 doi:10.20944/preprints202307.0958.v1

Disclaimer/Publisher's Note: The statements, opinions, and data contained in all publications are solely those of the individual author(s) and contributor(s) and not of MDPI and/or the editor(s). MDPI and/or the editor(s) disclaim responsibility for any injury to people or property resulting from any ideas, methods, instructions, or products referred to in the content.

Article

Large-Range Switchable Asymmetric Transmission and Circular Conversion Dichroism in a VO_2 Based Metasurface

Songliang Zhao [1], Huan Jiang [1,2,*], Jingyu Wang [1], Wenchang Zhu [1] and Weiren Zhao [1,*]

[1] School of Physics and Optoelectronic Engineering, Guangdong University of Technology, Guangzhou 510006, China
[2] Guangdong Provincial Key Laboratory of Information Photonics Technology, Guangdong University of Technology, Guangzhou 510006, China
* Correspondence: Jianghuan@gdut.edu.cn (H.J.); zwrab@163.com (W.Z.)

Abstract: Reconfigurable chiral metasurfaces with dynamic polarization manipulation capability are highly required in optical integrated systems. In this paper, we simultaneously realized giant and large-range switchable asymmetric transmission (AT) and circular conversion dichroism (CCD) in a vanadium dioxide (VO_2) based metasurface. The AT and CCD of the insulator VO_2 based metasurface reach 0.95 and 0.92, respectively. Utilizing the insulator-to-metallic phase transition of VO_2, the AT and CCD could be continuously switched to near zero. Furthermore, the physics mechanism of the giant and switchable AT and CCD are analyzed. The proposed metasurface with large-range switchable AT and CCD is promising in the applications of biochemistry detection, chiral imaging and biosensing.

Keywords: active metasurface; phase change materials; chiral effects; dynamic polarization control

1. Introduction

Chirality is defined as the characteristic for one object cannot be coincided with its mirror image [1], which has broad potential application prospects in chiral coding [2], analytical chemistry [3], chiral biosensing [4] and so on. Chiral effects, circular birefringence (CB) and circular dichroism (CD), are first found in three-dimension spiral structures while interacting with circular polarized light (CPL) [5]. However, these chiral effects are relatively weak in nature materials. Differently, chiral metasurfaces, artificially designed subwavelength optical structures, possess excellent performance in enhancing CB and CD. With the development of chiral metasurfaces, the two-dimension chiral effects of asymmetric transmission (AT) and circular conversion dichroism (CCD) are also obtained in planar symmetry broken structures [6]. Up to now, metasurfaces have been widely used to realize intrinsic [6] and extrinsic chirality [7] by breaking the symmetry of unit structure and oblique incidence, respectively. Unlike the extrinsic chirality at the expense of oblique incidence, intrinsic chirality could be realized in symmetry broken structures under normal incidence. For instance, Ahsan Sarwar Rana and Inki Kim et al. realized both AT (0.58) and CCD (0.55) in an asymmetric planar structure [8]. Similarly, both AT (0.8) and CD (0.88) are realized in a Z-shape germanium metasurface [6]. Although giant 2D chirality has been realized, the chiral effects of these metasurfaces are fixed once the structures are fabricated [9].

To attain dynamic chiral effects, some active materials including 2D materials graphene [10,11] and black phosphorus [7], phase change materials $Ge_2Sb_2Te_5$ (GST) [12,13] and VO_2 [14,15], liquid crystal [16] and ultrathin TiN films [17] are applied in traditional static metasurfaces. Among them, phase-change material VO_2 exhibits obvious phase transition behavior under the excitations of thermal [18], electrical [19,20] or optical [19] stimuli. With the phase transition from insulator to metallic state, the conductivity of VO_2 will change 4-5 orders of magnitudes. Besides, the lower phase-transition temperature (68 °C) of VO_2 than that of GST (160 °C) [12] shows the advantage of lower energy consumption. Benefit from these advantages, VO_2 has applied to construct reconfigurable

© 2023 by the author(s). Distributed under a Creative Commons CC BY license.

Preprints (www.preprints.org) | NOT PEER-REVIEWED | Posted: 14 July 2023 doi:10.20944/preprints202307.0958.v1

chiral metasurfaces. Lv et al. designed a bilayer twisted E-shape structure integrated with VO_2 and achieved strength-switchable AT and CD (0.6/0.45 ~0) [21]. Meng Liu et al. realized dynamic AT and CCD in a VO_2 based split rings structure and the AT/CCD ranges from 0.12/0.75 to near zero [22]. Though the strength-switchable AT and CCD have been realized, the switching ranges of these chiral effects are not broad enough, which will limit the application of chiral metasurfaces.

In this work, the giant and strength-switchable 2D chiral effects of AT and CCD are simultaneously achieved in a VO_2 based metasurface in THz region. The metasurface allows the transmission of RCP wave propagating along -z direction (forward) and prevents the propagation of RCP in z direction (backward), exhibiting AT effect as shown in Figure 1 (a). Meanwhile, the giant difference of cross-polarization reflection of LCP and RCP light indicates the existence of giant CCD in Figure 1(b). The maximum values of AT and CCD of the insulator VO_2 based metasurface are 0.95 and 0.92 at 0.69 THz. Furthermore, by thermally controlling the phase of VO_2, AT/CCD could be dynamically switched from 0.95/0.92 to near zero. The strength and the switching range of AT and CCD are much improved compared with previously reported works. The proposed metasurface with giant and switchable 2D chirality will promote the applications in optical imaging and chiral biosensing etc.

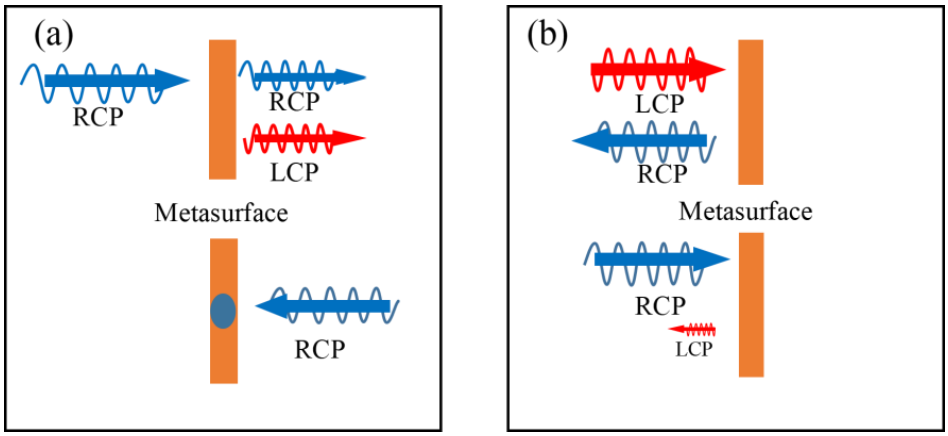

Figure 1. The dual functions of the proposed VO_2 based metasurface. (a) AT (b) CCD in reflection mode.

2. Design and simulations

It is widely used to break the structures' geometric symmetry in the wave propagation direction to generate chirality [23,24]. To break the symmetry of our structure, asymmetric G-shape and J-shape Au resonators are placed on the opposite sides of the VO_2 inserted polymer layer as shown in Figure 2. When VO_2 is insulator state, the incident CPL could polarization selectively penetrate and realize giant chiral effect. In contrast, the both incident CPL will be blocked when the VO_2 phase is changed to metallic state and show very weak chiral effect. Thus, utilizing the thermal tuning the properties of VO_2, the chiral effect of the VO_2 based reconfigurable metasurface could be modulated dynamically. The structure of the period array based on VO_2 with giant chiral effect is shown in Figure 2 (a). The structure marked by dashed frame in Figure 2 (a) is the unit structure. The top layer is the 90° rotated G-shaped Au resonator and the bottom layer is the 180° rotated J-shaped Au resonator as shown in Figure 2(c)(d). After optimization, the thickness of the Au resonators in both top and bottom layers is the same as $t_1 = 18\mu m$. The thickness of the separated polymers and inserted VO_2 layer are $t_2 = 19.7\mu m$ $t_3 = 20\mu m$ and $t_4 = 0.3\mu m$ as labeled in Figure 2 (b).

Preprints (www.preprints.org) | NOT PEER-REVIEWED | Posted: 14 July 2023 doi:10.20944/preprints202307.0958.v1

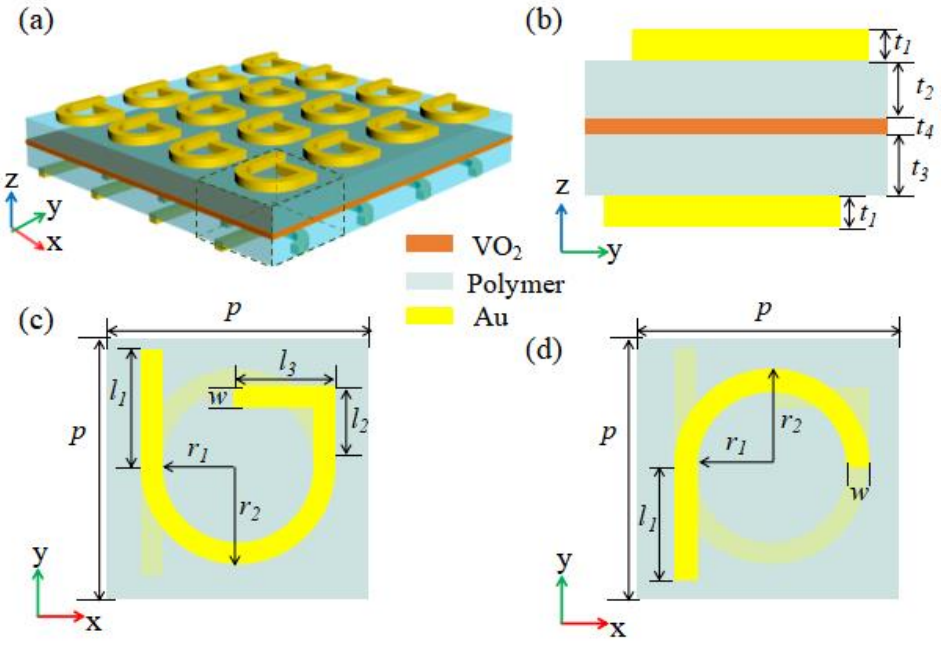

Figure 2. (a) The schematic illustration of the VO_2 based chiral metasurface. The (b) side, (c) top and (d) bottom views of the unit structure. The geometrical dimensions are $p=118\mu m$, $r_1=24\mu m$, $r_2=34\mu m$, $l_1=54\mu m$, $l_2=30\mu m$, $l_3=43\mu m$, $w=10\mu m$, $t_1=18\mu m$, $t_2=19.7\mu m$, $t_3=20\mu m$, $t_v=0.3\mu m$.

The optical property of Au substrate could be described by Drude model and the conductivity is set as $\sigma_{Au}=4.56\times10^7$ S/m [21]. The polymer spacer is regarded as lossy dielectric material with the permittivity of 3.5 + 0.00945i [25]. With the temperature change from room temperature to phase-transition temperature $T_c\approx68°c$, Drude model is used to characterize the permittivity of VO_2 in THz region as [18]

$$\varepsilon(\omega)=\varepsilon_\infty-\frac{\omega_p^2(\sigma)}{\omega^2+i\gamma\omega} \tag{1}$$

$$\omega_p^2(\sigma)=\frac{\sigma}{\sigma_0}\omega_p^2(\sigma_0) \tag{2}$$

where $\varepsilon_\infty=12$ is permittivity at infinite frequency. The permittivity of the VO_2 $\varepsilon(\omega)$ is determined by plasma frequency ω_p ($\omega_{p_0}=1.4\times10^{15}$ rad/s, $\sigma_0=3\times10^5$ S/m). Thus, the optical properties of VO_2 under different phases could be described by conductivities. Specially, with the insulator-to-metallic transition of VO_2, the conductivity of VO_2 increases from 200 s/m to 2×10^5 s/m. In simulation, we numerically calculated the transmission and reflection spectra by using finite element method (FEM) in frequency domain in CST Microwave Studio. The periodic boundary conditions are used in x and y directions and open boundary is applied in z direction. Mesh is set as adaptive tetrahedral grids.

3. Giant and switchable asymmetric transmission

The polarization transmission coefficient spectra of CPL propagating forward and backward are numerically calculated in Figure 3(a)(b). The four transmission coefficients of the CPL propagating forward are not coincided with each other. The right-to-left polarization transmission coefficient ($\vec{t}_{-+}$) and right-to-right one ($\vec{t}_{++}$) are higher than the other two coefficients ($\vec{t}_{+-}$ and $\vec{t}_{--}$) in the band of 0.65 - 0.8 THz as shown in Figure 3(a). Specially, the maximum values of RCP transmission coefficients $\vec{t}_{++}$ and $\vec{t}_{-+}$ reach 0.729 and 0.649 at 0.69 THz, while the LCP ones ($\vec{t}_{+-}$ and $\vec{t}_{--}$) approach to 0. Since the change of propagation direction will result in the exchange of two enantiomeric

Preprints (www.preprints.org) | NOT PEER-REVIEWED | Posted: 14 July 2023 doi:10.20944/preprints202307.0958.v1

arrangements, the subscripts "+" and "-" representing RCP and LCP will be exchanged, namely $\vec{t}_{++}=\overleftarrow{t}_{--}$, $\vec{t}_{--}=\overleftarrow{t}_{++}$, $\vec{t}_{+-}=\overleftarrow{t}_{-+}$, and $\vec{t}_{-+}=\overleftarrow{t}_{+-}$. The polarization transmission coefficients of CPL propagating in opposite directions are shown in Figure 3(b). The directions propagating forward and backward in transmission coefficients are represented by arrows "→" and "←", respectively. As expected, the co-polarization transmission coefficients propagating backward $\overleftarrow{t}_{--}(\overleftarrow{t}_{++})$ are the same as the forward ones $\vec{t}_{++}(\vec{t}_{--})$. Similarly, the cross-polarization transmission coefficients propagating backward $\overleftarrow{t}_{-+}(\overleftarrow{t}_{+-})$ and the forward ones $\vec{t}_{+-}(\vec{t}_{-+})$ are also the same.

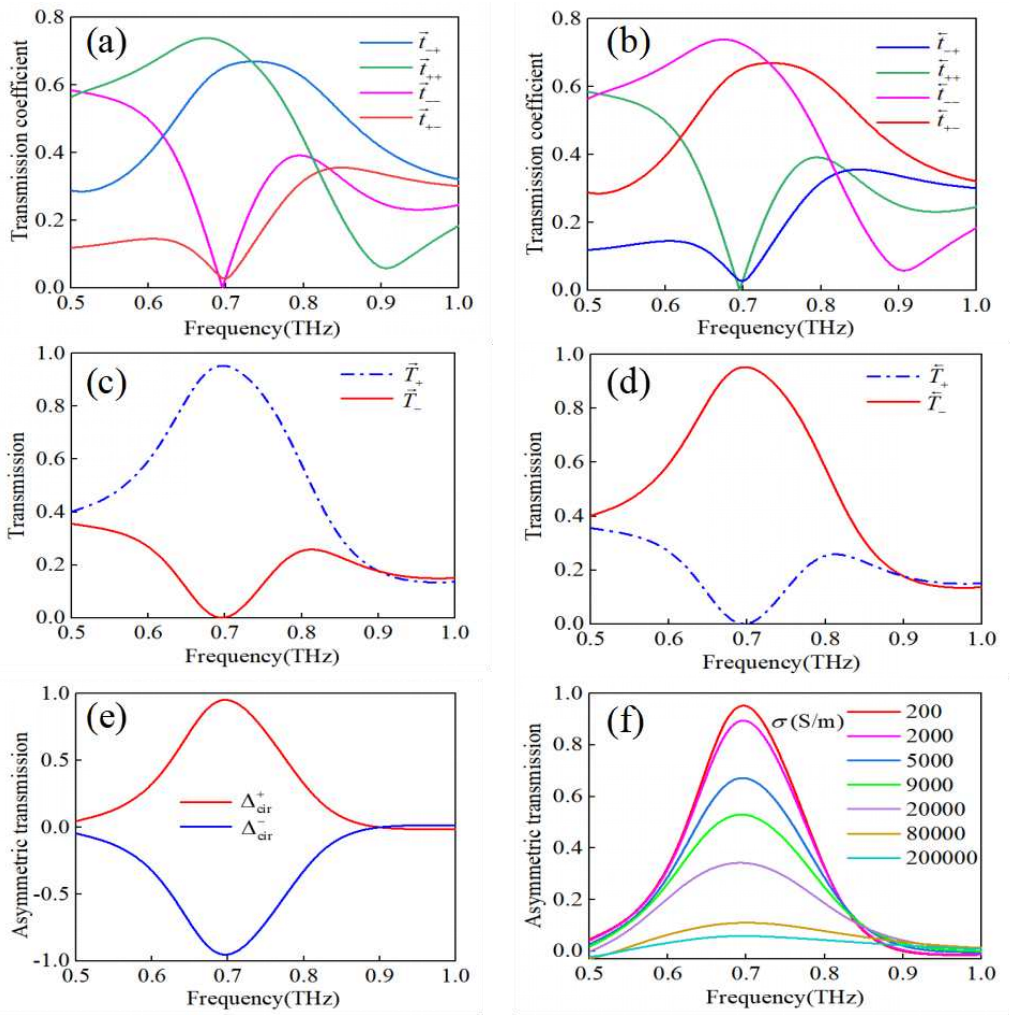

Figure 3. Giant and switchable AT. The transmission coefficient spectra of the CPL propagating (a) forward and (b) backward. The transmission of RCP and LCP propagating (c) forward and (d) backward. (e) AT parameters of RCP and LCP light. (f) Strength-switchable AT.

The transmission difference of the CPL propagating forward and backward is described as AT phenomenon [5]. To describe the transmission difference propagating in opposite directions, the transmission of CPL propagating forward and backward are separately calculated in Figure 4(c)(d). The polarization transmissions are derived from polarization transmission coefficients as $\vec{T}_{\pm}=\left|\vec{t}_{\mp\pm}\right|^2+\left|\vec{t}_{\pm\pm}\right|^2$ and $\overleftarrow{T}_{\pm}=\left|\overleftarrow{t}_{\mp\pm}\right|^2+\left|\overleftarrow{t}_{\pm\pm}\right|^2$. The transmission of RCP ($\vec{T}_{+}$) propagating forward are very high and the value of the value at peak is about 0.95 at 0.69 THz, but the ones of LCP $\vec{T}_{-}$ maintains low values and the dip value even approach to zero in Figure 3(c). As expected, the transmission of RCP/LCP light propagating forward is equal to the transmission of LCP/RCP propagating backward ($\vec{T}_{+}=\overleftarrow{T}_{-}$, $\vec{T}_{-}=\overleftarrow{T}_{+}$) as the curves shown in Figure 3(d). The transmission difference of RCP light

Preprints (www.preprints.org) | NOT PEER-REVIEWED | Posted: 14 July 2023 doi:10.20944/preprints202307.0958.v1

propagating forward and backward in Figure 3(c)(d) means the incident RCP light could transmit our metasurface forward but the RCP light from opposite direction will be blocked.

To estimate the giant AT performance quantitatively, the AT parameters of RCP and LCP light (Δ_{cir}^{+} and Δ_{cir}^{-}) are defined by the polarization transmission differences as [26]

$$\Delta_{cir}^{+} = \vec{T}_{+} - \overleftarrow{T}_{+} = \vec{T}_{+} - \vec{T}_{-} = \left|\vec{t}_{-+}\right|^2 + \left|\vec{t}_{++}\right|^2 - \left|\vec{t}_{+-}\right|^2 - \left|\vec{t}_{--}\right|^2 \tag{3}$$

$$\Delta_{cir}^{-} = \vec{T}_{-} - \overleftarrow{T}_{-} = \vec{T}_{-} - \vec{T}_{+} = \left|\vec{t}_{--}\right|^2 + \left|\vec{t}_{+-}\right|^2 - \left|\vec{t}_{-+}\right|^2 - \left|\vec{t}_{++}\right|^2 \tag{4}$$

As shown in Figure 3(e), the maximum AT parameter of RCP (Δ_{cir}^{+}) reaches 0.95 at 0.69 THz. Since the inversion relationship between polarization states and propagation direction, the AT parameters of LCP and RCP light are negative of each other ($\Delta_{\mathrm{cir}}^{-} = -\Delta_{\mathrm{cir}}^{+}$). The maximum absolute value of AT parameters for LCP is at 0.69 THz with $\Delta_{\mathrm{cir}}^{-} = -0.95$ Thus, the metasurface with giant AT parameter allows near perfect transmission of RCP light propagating forward and prevents that of LCP, which is corresponding to the RCP light propagating backward.

By controlling the phase of VO_2, the strength of AT effect could be continuously switched. As shown in Figure 3(f), when VO_2 is in insulator state (200 S/m), the metasurface exhibits giant AT effect (0.95) at 0.69 THz. But the AT will be disappeared when VO_2 is transformed into metallic state (2×10^5 S/m). The strength of AT could be dynamically switched in the broad switching range from 0.95 to 0.05. The VO_2 based chiral metasurface with giant and large-range switchable AT shows great potential in the fields of optical integrated system.

4. Giant and switchable circular conversion dichroism

Not only giant AT effect, the same nanostructure also shows great polarization selectivity for the reflection CPL. The reflection coefficient spectra of the CPL propagating forward and backward are displayed in Figure 4(a)(b). The co-polarized refection coefficients of both CPL propagating in two opposite directions are equal ($\vec{r}_{++} = \vec{r}_{--}$ and $\overleftarrow{r}_{++} = \overleftarrow{r}_{--}$) at 0.5-0.87 THz. Differently, the cross-polarized reflection coefficients are totally different. In detail, the left-to-right polarization reflection coefficient $\vec{r}_{+-}$ is much larger than the one of right-to-left one $\vec{r}_{-+}$ in Figure 4(a). Especially, the $\vec{r}_{+-}$ is as large as 0.96 at 0.69 THz while $\vec{r}_{-+}$ approaches to zero at the same frequency, which indicates the giant polarization selectivity of reflected light. In contrast, for the reflected light incident backward, the difference between cross-polarized reflection coefficients is not remarkable as shown in Figure 4(b).

To quantitatively characterize the giant difference of the cross-polarization reflection coefficients, CCD is calculated in Figure 4(c), which is defined by the difference of $\left|r_{+-}\right|^2$ and $\left|r_{-+}\right|^2$ as $CCD = \left|\vec{r}_{+-}\right|^2 - \left|\vec{r}_{-+}\right|^2$ [22]. The curves of $\left|\vec{r}_{+-}\right|^2$ and $\left|\vec{r}_{-+}\right|^2$ are not coincided in the whole frequency band and the maximum difference occurs at 0.69 THz with the values of $\left|\vec{r}_{+-}\right|^2 = 0.92$ and $\left|\vec{r}_{-+}\right|^2 \approx 0$ respectively. The maximum of CCD reaches 0.92 at 0.69 THz. The high CCD represents the giant difference between the cross-polarization conversion of incident LCP and RCP light.

The strength of CCD could be dynamically switched in the VO_2 based active metasurface. By unitizing the phase-transition of VO_2, the strength of CCD of metasurface is continuously controlled from 0.92 to ~0 at 0.69 THz in Figure 4(d). In details, with the conductivity increasing from 200 S/m (insulator VO_2) to 2×10^5 S/m (metallic VO_2), the CCD value is gradually decreased in a broad range at 0.69 THz. The broad-range and continuous switching for CCD is a major advance when compared with the previously reported works.

Preprints (www.preprints.org) | NOT PEER-REVIEWED | Posted: 14 July 2023 doi:10.20944/preprints202307.0958.v1

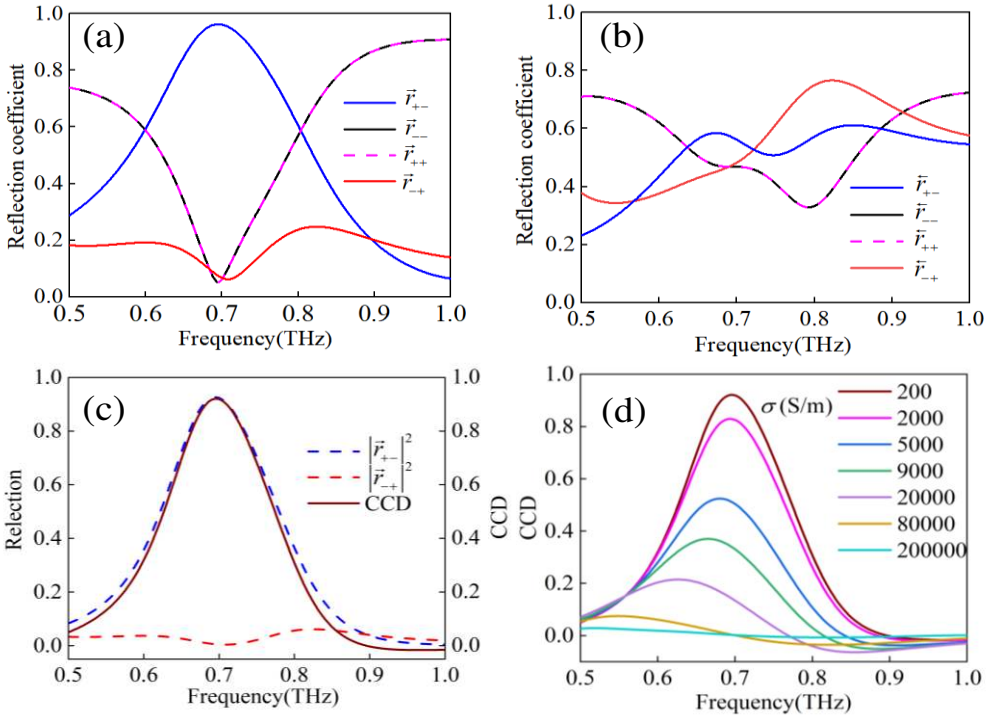

Figure 4. Giant and switchable CCD effect. Reflection coefficients spectra incident (a) forward and (b) backward. (c) The cross-polarization reflection coefficients and CCD spectra. (d) The strength switchable CCD by tuning the phase of VO_2.

5. The principle of chiral effects

To explore the physic mechanism of AT and CCD, the electric field and surface current distributions of the chiral metasurface at 0.69 THz are given out in Figure 5. As mentioned, the metasurface with insulator VO_2 exhibits different polarization responses for RCP and LCP light. The incident RCP light could penetrate metasurface as the homogeneous electric field distributed above and below the metasurface in Figure 5(a). In contrast, the incident LCP light will be reflected which leads to obvious difference of electric filed distributions above and below the metasurface as shown in Figure 5(b). The huge difference in transmission and reflection of RCP and LCP light exhibits remarkable AT and CCD effects.

To explain the mechanism of different responses for RCP and LCP light, the surface current distributions in the top and bottom layers are shown in Figure 5(e)(f)(i)(j). Under the excitation of RCP light, there are enhanced parallel and circular surface currents in the top layer as shown in Figure 5(e). In detail, the parallel surface current points to -y direction and the circular surface current flows clockwise. As known, electric dipole resonance is characterized by parallel surface current flowing from one pole to another pole and magnetic dipole resonance is characterized by circular surface currents [27]. Thus, with incidence of RCP light, the electric current marked by arrows shows the excitations of electric (E_t) and magnetic (M_t) dipole resonances in the top layer in Figure 5(e). Similarly, electric and magnetic dipole resonances could be simultaneously excited in the bottom layer (Figure 5(i)).

In contrast, with LCP light incidence, the electric and magnetic dipole resonances could also be excited in Figure 5(f)(j), but electric moment pointing in opposite directions as the black arrows marked in the both layers in comparisons (Figure 5(e) and Figure 5(f), Figure 5(i) and Figure 5(j)). Differently, the directions of electric moment is reversed at the same geometric position in the top and bottom layers under LCP excitation compared with RCP excitation. It is worth noting that the intensity of surface current under LCP excitation is generally enhanced than that of RCP excitation. Because the variation of resonance modes and surface current intensity will result in the different responses for RCP and LCP and generate giant AT and CCD in the metasurface with insulator VO_2.

Preprints (www.preprints.org) | NOT PEER-REVIEWED | Posted: 14 July 2023 doi:10.20944/preprints202307.0958.v1

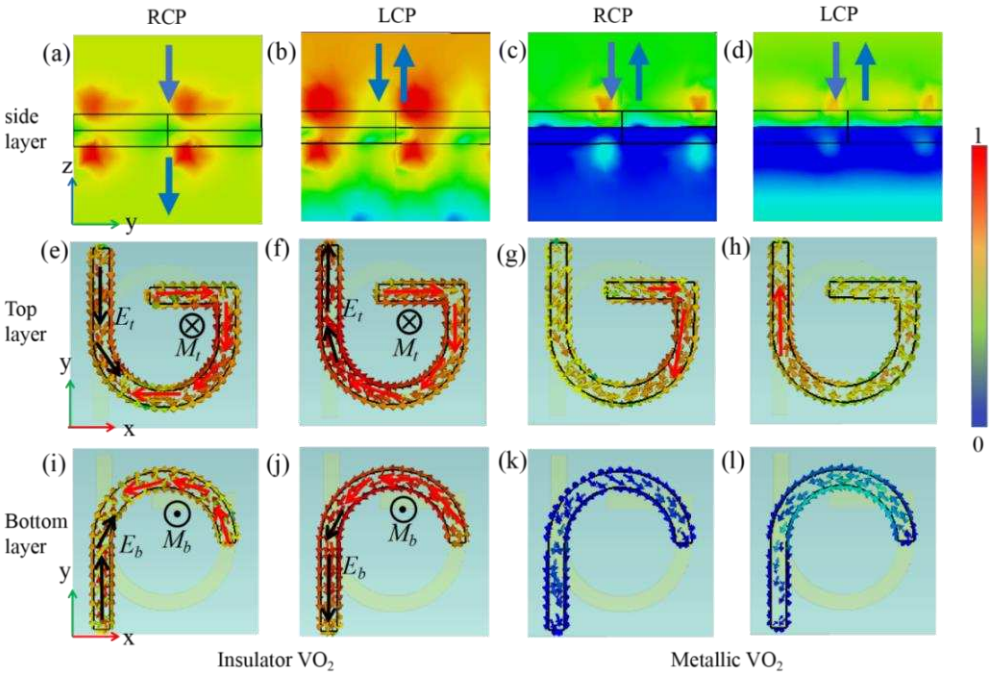

Figure 5. The electric field and surface current distributions at 0.69 THz. With (a)(b)(e)(f)(i)(j) insulator and (c)(d)(g)(h)(k)(l) metallic VO_2, (a)-(d) the electric fields at the side layers and (e)-(l) surface current at the (e)-(h) top and (i)-(l) bottom layers excited by (a)(e)(i)(c)(g)(k) RCP and (b)(f)(j) (d)(h)(l) LCP light.

By changing the phase of VO_2, both the values of AT and CCD could be continuously switched to near zero. When VO_2 undergoes insulator-to-metallic transition, the incident CPL could hardly penetrate the metallic VO_2 and excites very weak electric field and surface current in the bottom layer as shown in Figure 5(g)(h)(k)(l). The difference of electric and magnetic resonance modes and surface current are unremarkable under the excitations of RCP and LCP light, which results in the weak response difference between RCP and LCP light. Thus, when the VO_2 is changed to metallic state, the 2D chiral effect including AT and CCD almost could not be excited in the same nanostructure and achieves large-range dynamic switching.

Here, we compare the chiral performances of our chiral structure with previously reported works in Table 1. The first three works have realized prominent but fixed chiral effects. The latter two works could realize active manipulation for AT and CCD/CD by integrating VO_2, but the switching range are not large enough. In contrast, not only the stronger AT (0.95)/CCD (0.92) are obtained but also the larger-range switching for 2D chirality from ~1 to ~0 are realized by controlling the phase states of VO_2. The proposed chiral metasurfaces with simultaneous giant AT/CCD and broad range switching capability for chirality are essential for the applications of polarization filtering, polarization optical isolating and so on.

Table 1. The comparison with reported chiral metasurfaces.

Nano-structures	Bandwidths	AT	CCD/CD	Switching capability	Active materials	Years
Nano-fifin design [8]	500-800 nm	0.58	CCD=0.55	No	/	2020
Z-shape [28]	3.0-8.0 GHz	0.38	CD=0.75	No	/	2021
Twisted S-shaped structure [23]	0.4-2.0 THz	0.73	CD=0.28	No	/	2020
Double-layered arcs [29]	0.8-1.5 μm	0.15	CD=0.7	Yes	VO_2	2021
Split rings [22]	0.4-0.8 THz	0.12	CCD=0.75	Yes	VO_2	2020
"G"- and "J"- shaped hybrid structure	**0.5-1.0 THz**	**0.95**	**CCD=0.92**	**Yes**	**VO_2**	**This work**

Preprints (www.preprints.org) | NOT PEER-REVIEWED | Posted: 14 July 2023 doi:10.20944/preprints202307.0958.v1

6. Conclusions

In conclusion, we numerically achieved giant and strength-switchable AT and CCD in a VO_2 based chiral metasurface by breaking the geometric symmetry of structures in the wave propagation direction. The giant AT parameter (0.95) and CCD (0.92) are realized in THz region, which is much improved compared with the proposed chiral metasurfaces. Furthermore, the strength of the AT and CCD effect are large-range switched from ~ 1 to ~0 by thermally controlling VO_2. The physical mechanism of the giant and reconfigurable AT and CCD are analyzed by surface current distributions. The giant chirality originates from the polarization selective excitations of electric and magnetic dipole resonances. The proposed active metasurface with broad switchable range for both AT and CCD will promote the development of integration chiral devices.

Supplementary Materials: The following supporting information can be downloaded at the website of this paper posted on Preprints.org. Figure 1. The dual functions of the proposed VO_2, Figure 2. (a) The schematic illustration of the VO_2 based chiral metasurface, Figure 3. Giant and switchable AT, Figure 4. Giant and switchable CCD effect. Figure 5. The electric field and surface current distributions at 0.69 THz.

Author Contributions: All authors contributed to the study's conception and design. Theoretical analysis, structure simulation, date collection were performed by Songliang Zhao, Huan Jiang, Jingyu Wang, Wenchang Zhu and Weiren Zhao. Data processing and graph drawing were carried out Songliang Zhao and Huan Jiang. The first draft of manuscript is written by Songliang Zhao. All the authors read and approved the finial manuscript.

Funding: National Natural Science Foundation of China (12004080); Funding by Science and Technology Projects in Guangzhou (202201010540).

Data Availability Data underlying the results presented in this paper are not publicly available at this time but may be obtained from the authors upon reasonable request.

Conflicts of Interest: The authors declare no conflicts of interest.

References

1. Hwang J, Song M H, Park B et al Electro-tunable optical diode based on photonic bandgap liquid-crystal heterojunctions. Nat Mater **2005**, 4 383-387.
2. Li Z, Jiang C, Wang K et al Active manipulation of Dirac semimetals supported chiral coding metasurfaces for multifunctional applications in terahertz region. Results in Physics **2023**, 46.
3. Valev V K, Baumberg J J, Sibilia C et al Chirality and chiroptical effects in plasmonic nanostructures: fundamentals, recent progress, and outlook. Adv Mater **2013**, 25, 2517-2534.
4. Zhan P, Dutta P K, Wang P et al Reconfigurable Three-Dimensional Gold Nanorod Plasmonic Nanostructures Organized on DNA Origami Tripod. ACS Nano **2017,** 11, 1172-1179.
5. L. D. Barron, Molecular light scattering and optical activity (Cambridge University Press, **2009**).
6. Ma Z, Li Y, Li Y et al All-dielectric planar chiral metasurface with gradient geometric phase. Opt Express **2018**, 26, 6067-6078.
7. Zeng Y, Xu J, Xiao W et al Giant 2D-chiroptical response in an achiral metasurface integrated with black phosphorus. Opt Express **2022**, 30, 8266-8274.
8. Rana A S, Kim I, Ansari M A et al Planar Achiral Metasurfaces-Induced Anomalous Chiroptical Effect of Optical Spin Isolation. ACS Appl Mater Interfaces **2020**, 12, 48899-48909.
9. Shi T, Deng Z L, Geng G et al Planar chiral metasurfaces with maximal and tunable chiroptical response driven by bound states in the continuum. Nat Commun **2022,** 13, 4111.
10. Cui Y, Wang X, Jiang H et al High-efficiency and tunable circular dichroism in chiral graphene metasurface. Journal of Physics D: Applied Physics **2021** 55.
11. Tao X, Qi L, Fu T et al A tunable dual-band asymmetric transmission metasurface with strong circular dichroism in the terahertz communication band. Optics & Laser Technology **2022,** 150.
12. Jiang H, Peng K Z, Cui Y et al Design and simulation of a GST-based metasurface with strong and switchable circular dichroism. Opt Lett **2022**, 47, 1907-1910.
13. Dong G, Qin C, Lv T et al Dynamic chiroptical responses in transmissive metamaterial using phase-change material. Journal of Physics D: Applied Physics **2020,** 53.

Preprints (www.preprints.org) | NOT PEER-REVIEWED | Posted: 14 July 2023 doi:10.20944/preprints202307.0958.v1

14. Lv T, Li Y, Qin C et al Versatile polarization manipulation in vanadium dioxide-integrated terahertz metamaterial. Opt Express **2022**, 30, 5439-5449.
15. Yang J-K, and Jeong H-S Switchable Metasurface with VO_2 Thin Film at Visible Light by Changing Temperature. Photonics **2021**, 8.
16. Baranzadeh F, and Nozhat N High Performance Plasmonic Nano-Biosensor Based on Tunable Ultra-Narrowband Perfect Absorber Utilizing Liquid Crystal. Plasmonics **2020**, 16, 253-262.
17. Qin F, Chen X, Yi Z et al Ultra-broadband and wide-angle perfect solar absorber based on TiN nanodisk and Ti thin film structure. Solar Energy Materials and Solar Cells **2020**, 211.
18. Wen Q-Y, Zhang H-W, Yang Q-H et al Terahertz metamaterials with VO_2 cut-wires for thermal tunability. Applied Physics Letters **2010**, 97.
19. Zhang C, Zhou G, Wu J et al Active Control of Terahertz Waves Using Vanadium-Dioxide-Embedded Metamaterials. Physical Review Applied **2019**, 11.
20. Butakov N A, Knight M W, Lewi T et al Broadband Electrically Tunable Dielectric Resonators Using Metal–Insulator Tranitions. ACS Photonics **2018**, 5, 4056-4060.
21. Lv T T, Li Y X, Ma H F et al Hybrid metamaterial switching for manipulating chirality based on VO_2 phase transition. Sci Rep **2016**, 6 23186.
22. Liu M, Plum E, Li H et al Switchable Chiral Mirrors. Advanced Optical Materials **2020,** 8.
23. Lv T, Chen X, Dong G et al Dual-band dichroic asymmetric transmission of linearly polarized waves in terahertz chiral metamaterial. Nanophotonics **2020**, 9, 3235-3242.
24. Luo C, Sang T, Li S et al Stretchable Chiral Metamaterial for Flexible Control of Broadband Asymmetric Transmission. Plasmonics **2022**, 18, 29-37.
25. Hu F, Wang L, Quan B et al Design of a polarization insensitive multiband terahertz metamaterial absorber. Journal of Physics D: Applied Physics **2013**, 46.
26. Singh R, Plum E, Menzel C et al Terahertz metamaterial with asymmetric transmission. Physical Review B **2009**, 80.
27. Jiang H, Zhao W, and Jiang Y All-dielectric circular polarizer with nearly unit transmission efficiency based on cascaded tensor Huygens surface. Opt Express **2016**, 24, 17738-17745.
28. Han B, Li S, Li Z et al Asymmetric transmission for dual-circularly and linearly polarized waves based on a chiral metasurface. Opt Express **2021**, 29, 19643-19654.
29. Ren Y, Zhou T, Jiang C et al Thermally switching between perfect absorber and asymmetric transmission in vanadium dioxide-assisted metamaterials. Opt Express **2021**, 29, 7666-7679.

Disclaimer/Publisher's Note: The statements, opinions and data contained in all publications are solely those of the individual author(s) and contributor(s) and not of MDPI and/or the editor(s). MDPI and/or the editor(s) disclaim responsibility for any injury to people or property resulting from any ideas, methods, instructions or products referred to in the content.